

# Surface Studies of Aqueous Methanol Solutions by Vibrational Broad Bandwidth Sum Frequency Generation Spectroscopy

Gang Ma and Heather C. Allen\*

Department of Chemistry, The Ohio State University, 100 West 18th Avenue, Columbus, Ohio 43210

Received: October 31, 2002; In Final Form: April 9, 2003

Neat methanol ( $\text{CH}_3\text{OH}$ ) and aqueous methanol solutions were investigated using broad bandwidth sum frequency generation (BBSFG), Raman spectroscopy, and FTIR spectroscopy. BBSFG results indicate a net orientation of methanol molecules at the air–liquid interfaces of neat methanol and aqueous methanol solutions. However, as the methanol concentration increases above 0.57 methanol mole fraction the methanol molecules become less ordered, i.e., a larger distribution of orientation angles of the  $\text{CH}_3$  transition moment about the surface normal exists. This was further verified by the BBSFG results from partially deuterated methanol ( $\text{CD}_3\text{OH}$ ) aqueous solutions. A red-shift of the  $\text{CH}_3$  symmetric stretch ( $\text{CH}_3$ –SS) frequency with the increase of methanol concentration observed by BBSFG, Raman, and FTIR spectroscopy suggests a changing hydrogen-bonding configuration between the methanol and the water molecules at the surface and in the bulk. Moreover, the surface studies strongly suggest that methanol is a more efficient hydrogen-bonding acceptor when the methanol molecule resides in the interfacial region.

## Introduction

Oxygenated hydrocarbons play an important role in the upper troposphere.<sup>1,2</sup> These species impact not only the  $\text{HO}_x$  cycle, but also  $\text{NO}_y$  reactions in this atmospheric region.<sup>3</sup> However, the sources and sinks of these oxygenated hydrocarbons are not well understood. For example, methanol was found to be less abundant than acetone in the upper troposphere, implying possible heterogeneous reaction sinks for methanol.<sup>4</sup> Such heterogeneous reactions may occur on the surfaces of aerosols and ice crystals in cirrus clouds.<sup>5</sup> Since surface reactivity of chemical species to a great extent is influenced by surface structure, fundamental studies elucidating the orientation and structure of the molecules residing at surfaces are necessary and helpful for understanding heterogeneous atmospheric processes.

In the studies presented here, Raman, FTIR, and vibrational broad bandwidth sum frequency generation (BBSFG) spectroscopy are used to investigate the liquid phase and the air–liquid interface of aqueous methanol solutions, respectively. As a surface-sensitive spectroscopic technique, sum frequency generation (SFG) has been used to study a variety of surfaces and interfaces relevant to surface science and material science.<sup>6–12</sup> In recent years, the application of SFG in laboratory studies of atmospheric heterogeneous processes has been gaining prominence.<sup>13–17</sup> Under the electric-dipole approximation, SFG is a forbidden process in isotropic bulk media, yet is allowed at surfaces and interfaces due to the lack of inversion symmetry within the boundary between the two media. Therefore, SFG is a surface-selective technique. Furthermore, the vibration-resolvable ability of infrared-visible SFG makes surface vibrational signatures obtainable.

The theory of SFG has been described previously.<sup>18–25</sup> However, a brief overview of SFG theory is presented here.

The SFG intensity,  $I_{\text{SFG}}$ , as shown in eq 1,

$$I_{\text{SFG}} \propto |\chi^{(2)}|^2 \propto |\chi_{\text{NR}}^{(2)} + \sum_v \chi_v^{(2)}|^2 \quad (1)$$

is proportional to the absolute square of the macroscopic second-order nonlinear susceptibility,  $\chi^{(2)}$ , which consists of resonant terms ( $\chi_v^{(2)}$ )

$$\chi_v^{(2)} \propto \frac{A_v}{\omega_v - \omega_{\text{IR}} - i\Gamma_v} \quad (2)$$

and a nonresonant term ( $\chi_{\text{NR}}^{(2)}$ ). When the frequency of an incident infrared beam,  $\omega_{\text{IR}}$ , is resonant with a surface vibrational mode,  $v$ , the resonant susceptibility term ( $\chi_v^{(2)}$ ) dominates the nonlinear susceptibility ( $\chi^{(2)}$ ) and a SFG intensity enhancement is observed. The resonant macroscopic nonlinear susceptibility,  $\chi_v^{(2)}$ , is shown in eq 2, where  $A_v$  is the strength of the transition moment,  $v$  is the frequency of the transition moment, and  $\Gamma_v$  is the line-width of the transition. The amplitude,  $A_v$ , is nonzero when the Raman and the infrared transitions are spectroscopically allowed.  $\chi_v^{(2)}$  is related to the molecular hyperpolarizability,  $\beta_v$ , shown in eq 3, by the number density of surface species,

$$\chi_v^{(2)} = N \sum_{lmn} \langle \mu_{IJK:lmn} \rangle \beta_v \quad (3)$$

$N$ , and an orientationally averaged Euler angle transformation,  $\langle \mu_{IJK:lmn} \rangle$ , between the laboratory-coordinates ( $I, J, K$ ) and the molecule-coordinates ( $l, m, n$ ).

SFG is generally performed by combining one narrow bandwidth visible laser pulse with one narrow bandwidth infrared (IR) laser pulse. By scanning the frequency of the IR beam across the vibrational region of interest, a surface vibrational spectrum can be obtained if the incident IR photon is resonant with a vibrational mode of the molecules at the

\* Corresponding author. E-mail: allen@chemistry.ohio-state.edu.

surface. In the present study, femtosecond broad bandwidth technology is employed. The BBSFG system utilizes a broad bandwidth IR beam ( $\sim 100$  fs pulse duration) rather than a narrow bandwidth beam as is used in scanning SFG technologies. Therefore, scanning of the infrared frequency is not necessary. Because the vibrational SFG spectrum can be obtained within one laser pulse and because of the short duration of the infrared pulse, BBSFG spectroscopic systems can offer shorter acquisition times, larger SFG responses, and typically better signal-to-noise ratios than many scanning SFG systems.

In the present paper, the surface structure relative to the liquid-phase structure of methanol molecules as a function of methanol concentration in water is investigated using BBSFG, Raman, and FTIR spectroscopy, respectively.

## Experimental Section

The BBSFG system utilized here has been described previously.<sup>26,27</sup> Recently, a number of modifications have been made to this system and therefore a brief description is given. The BBSFG system consists of two regenerative amplifiers (Spectra-Physics Spitfire, fs and ps versions), both of which are seeded by splitting one sub-50 fs 800 nm pulse from a Ti:sapphire oscillator (Spectra-Physics, Tsunami). The oscillator is pumped by 4.7 W from a Nd:YVO<sub>4</sub> CW laser (Spectra-Physics, Millennia Vs, 532 nm). The regenerative amplifiers are pumped by an all solid-state Nd:YLF laser (Spectra-Physics, Evolution 30, 527 nm); 8.7 W and 11.5 W are used in the fs and ps regenerative amplifiers, respectively. The all solid-state Nd:YLF replaced the flash lamp-pumped Nd:YLF that was used in previous studies.<sup>26,27</sup> This system modification has substantially improved the hour-to-hour and day-to-day stability of the laser system. The two 1-kHz repetition rate regenerative amplifiers provide 85 fs pulses at 800 nm (22 nm bandwidth) and 2 ps pulses at 800 nm (17  $\text{cm}^{-1}$  bandwidth). The fs broad bandwidth pulses are then used to generate broad bandwidth infrared ( $\sim 600$   $\text{cm}^{-1}$  bandwidth) light via an optical parametric amplifier (Spectra-Physics, OPA-800CF). Tuning the BBO and AgGaS<sub>2</sub> crystals in the OPA allows one to cover different IR wavelength regions.

To narrow the output bandwidth of the 2 ps 800 nm beam to improve the spectral resolution of the BBSFG system, the compressor of the regenerative amplifier (ps version) was modified. A beam blocker is positioned in the compressor to partly block the spatially dispersed beam from the compressor grating and allows only a small spectral portion of the dispersed beam to be compressed. This modification spectrally narrows the output beam bandwidth of the formerly 2 ps 800 nm beam from 17  $\text{cm}^{-1}$  to  $\sim 5$   $\text{cm}^{-1}$ . The pulse width of the spectrally narrowed 800 nm beam was measured to be  $\sim 6$  ps by a single shot autocorrelator. The SFG experiment was then performed in reflection geometry using the narrow bandwidth (5  $\text{cm}^{-1}$ ) 800 nm beam (120  $\mu\text{J}$ ) and the broad bandwidth infrared beam (10  $\mu\text{J}$ ). (When investigating the C–D stretch region, 170  $\mu\text{J}$  of 796 nm and 6.5  $\mu\text{J}$  of infrared energy were used.) The broadband infrared and narrowband 800 nm pulses, which were incident on the sample at 66° and 58° from the surface normal, respectively, were overlapped at the sample surface spatially and temporally to produce a vibrationally resonant SFG spectrum. The SFG photons were emitted at 59.3° from the surface normal and were detected using a monochromator-CCD detection system (Acton Research, SpectraPro SP-500 monochromator; Roper Scientific, 1340  $\times$  400 pixel array, LN400EB back-illuminated CCD) with a 1200 g/mm grating blazed at 750

nm. The polarization combination for these studies was ssp (s: SFG, s: 800 nm, p: infrared). The nonresonant SFG spectrum from a GaAs (Lambda Precision Optics, Inc) crystal surface was obtained both with and without a polystyrene film covering the OPA infrared output port. The resulting SFG spectra were used for normalization purposes and as a reference to calibrate the peak positions of the BBSFG spectra. When investigating CD<sub>3</sub>OH systems, the CO<sub>2</sub> absorption peak in the nonresonant SFG spectrum from GaAs was used as a calibration reference. The BBSFG spectra were taken with 1-minute CCD acquisition times for the CH<sub>3</sub>OH systems and 10-seconds for the CD<sub>3</sub>OH systems at an ambient temperature of 23 °C.

Spectrophotometric grade methanol (CH<sub>3</sub>OH) (99.9%) obtained from Aldrich, methanol-*d*<sub>3</sub> (CD<sub>3</sub>OH) (99.5%) obtained from Cambridge Isotope Laboratories, Inc., and Nanopure water of 18 M $\Omega$  resistivity were used to make aqueous methanol solutions. A 1-in. diameter sample dish was utilized. The level of the air–liquid interface was set at the position of the beam overlap point using a *z*-axis positioner. Since the methanol vapor ( $V_{\text{P, methanol}}$  at 295 K is  $\sim 108$  Torr) in the air can absorb a portion of the incident IR beam, there is a possibility of introducing spectral artifacts. After evaluation of several closed and open sample cells and comparison of these spectra with background spectra, absorption and evaporation loss were minimized by using a 1-in. diameter dish open to the atmosphere for the duration of the acquisition time. The IR absorption by methanol vapor was less than 5%. The BBSFG spectrum from neat methanol (CH<sub>3</sub>OH) solution surface is consistent with previously published spectra both from a closed sample cell<sup>28</sup> and a cell open to the laboratory atmosphere.<sup>29</sup>

The Raman experimental setup consists of a 532 nm CW laser (Spectra-Physics, Millennia II), a 5 mm focusing Raman Probe (InPhotonics, RP 532-05-15-FC.), a 500-mm monochromator (Acton Research, SpectraPro SP-500) using a 600 g/mm grating and a back-illuminated CCD (Roper Scientific, LN400EB, 1340  $\times$  400 pixel array and deep depletion). The illumination fiber optic of the Raman probe was positioned in a home-built sample/test tube housing and the Raman backscatter was collected through the collection fiber optic after passing through the detection optics. The output end of the collection fiber was mounted to the entrance slit of the monochromator. SpectraSense software (Acton Research version 4.0.6) was used for data collection and display. The power of the 532 nm beam for sample illumination was 120 mW. The Raman spectral resolution was 0.78  $\text{cm}^{-1}$ . Before data collection, the Raman system was calibrated by using the 435.83 nm line of a fluorescence lamp, and the calibration was also verified by comparison to the Raman spectrum of naphthalene.

Infrared spectra were taken with 4  $\text{cm}^{-1}$  resolution and 128 scans by using a Thermal Nicolet Avatar 370 FT-IR spectrometer. A demountable liquid cell equipped with CaF<sub>2</sub> windows was utilized. Second-derivative technique was employed to determine the C–H stretch peak position.

Surface tensions were measured using a surface tensiometer (DeltaPi, Kibron Inc., Finland), which employs the Wilhelmy method. Values are averages of 10 measurements.

## Results and Discussion

The Raman spectrum in the CH region obtained from a neat methanol solution is shown in Figure 1. The 2835  $\text{cm}^{-1}$  peak is assigned to the CH<sub>3</sub> symmetric stretch (CH<sub>3</sub>-SS); the 2921  $\text{cm}^{-1}$  shoulder and the 2944  $\text{cm}^{-1}$  peak are assigned to the Fermi resonances (CH<sub>3</sub>-FR) of the CH<sub>3</sub> symmetric stretch with the overtones of the CH<sub>3</sub> bending mode.<sup>30,31</sup> The shoulder on the

**TABLE 1: Fitting Results of the Raman Spectra in the C–H Stretch Region of Aqueous Methanol (CH<sub>3</sub>OH) Solutions<sup>a</sup>**

mole fraction	CH <sub>3</sub> -SS				CH <sub>3</sub> -FR (1); CH <sub>3</sub> -FR (2)				CH <sub>3</sub> -AS			
	$\nu$ (cm <sup>-1</sup> )	$A_\nu$ (a.u.)	$I_\nu$ (a.u.)	HHWM (cm <sup>-1</sup> )	$\nu$ (cm <sup>-1</sup> )	$A_\nu$ (a.u.)	$I_\nu$ (a.u.)	HHWM (cm <sup>-1</sup> )	$\nu$ (cm <sup>-1</sup> )	$A_\nu$ (a.u.)	$I_\nu$ (a.u.)	HHWM (cm <sup>-1</sup> )
0.03	2846	0.024	0.45	9	2925; 2953	0.002; 0.037	0.063; 0.86	15; 12	2995	0.006	0.25	19
0.06	2845	0.055	1.27	10	2924; 2953	0.007; 0.062	0.26; 1.71	15; 12	2994	0.012	0.43	19
0.14	2844	0.12	3.03	11	2930; 2953	0.024; 0.12	1.37; 3.21	24; 12	2992	0.027	1.46	25
0.19	2843	0.17	4.10	11	2928; 2952	0.035; 0.15	1.87; 4.21	23; 12	2991	0.031	1.82	25
0.36	2841	0.28	6.90	11	2930; 2950	0.073; 0.22	4.40; 6.26	28; 12	2988	0.056	3.57	29
0.57	2838	0.39	9.74	11	2925; 2948	0.12; 0.22	6.71; 6.51	27; 12	2983	0.10	6.43	32
0.69	2837	0.45	10.92	10	2925; 2947	0.16; 0.24	7.96; 7.17	28; 12	2981	0.12	7.17	33
0.83	2836	0.57	12.51	10	2922; 2946	0.14; 0.28	7.92; 8.63	27; 13	2980	0.12	8.91	37
1.0	2835	0.59	13.25	10	2921; 2944	0.15; 0.27	8.35; 7.81	27; 12	2974	0.15	11.47	40

<sup>a</sup>  $\nu$ : peak frequency;  $A_\nu$ : peak amplitude;  $I_\nu$ : peak intensity (integrated peak area); HHWM: half width at half-maximum.

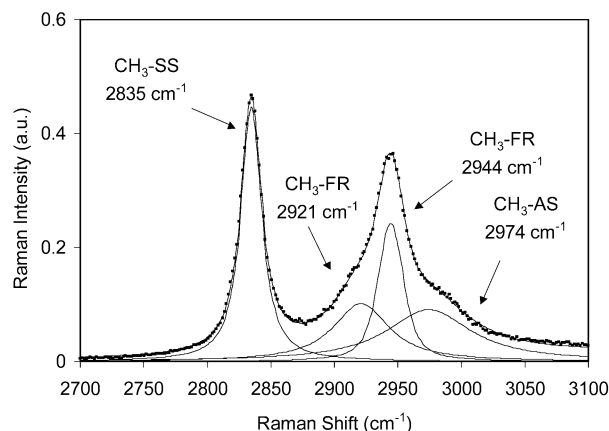


**Figure 1.** Raman spectrum of neat methanol (CH<sub>3</sub>OH). CH<sub>3</sub>-SS: CH<sub>3</sub> symmetric stretch; CH<sub>3</sub>-FR: CH<sub>3</sub> Fermi resonance; CH<sub>3</sub>-AS: CH<sub>3</sub> asymmetric stretch. The solid lines are the calculated Voigt fits.

high energy side of the 2944 cm<sup>-1</sup> peak shown at 2974 cm<sup>-1</sup> is assigned to the CH<sub>3</sub> asymmetric stretch (CH<sub>3</sub>-AS) modes. The CH<sub>3</sub>-SS and CH<sub>3</sub>-AS assignments are consistent with previously published infrared data.<sup>32</sup> The alternative assignments for the 2921 cm<sup>-1</sup> and the 2944 cm<sup>-1</sup> peaks are to the overtone of the CH<sub>3</sub> bending mode and to the CH<sub>3</sub> asymmetric stretch as opposed to the Fermi resonance assignments.<sup>32,33</sup> However, these peak assignments, 2921 and 2944 cm<sup>-1</sup>, continue to be debated among various research groups, experimental and theoretical.<sup>34</sup> Peak fits using Voigt functions (IGOR, version 4.0.5.1) for the Raman spectrum are also shown in Figure 1, the individual peaks and the additive calculated spectrum. The fitting parameters are listed in Table 1. Both Voigt and Lorentzian line shapes were tested for the best spectral fit. The Voigt profile was superior to a Lorentzian profile for this Raman spectrum.

The BBSFG spectrum in the CH region using ssp polarizations was obtained from the air–liquid interface of neat methanol and is shown in Figure 2. The spectral shape of this spectrum is consistent with previously published SFG spectra of neat methanol using scanning SFG systems.<sup>28,29</sup> The BBSFG spectrum shown in Figure 2 reveals two peaks and one shoulder on the low energy side of the smaller of the two peaks. Consistent with the Raman assignments, the observed peak at 2834 cm<sup>-1</sup> (peak fit at 2836 cm<sup>-1</sup>) is attributed to the CH<sub>3</sub>-SS. The observed peaks at 2912 cm<sup>-1</sup> (peak fit at 2917 cm<sup>-1</sup>) and 2946 cm<sup>-1</sup> (peak fit at 2948 cm<sup>-1</sup>) are attributed to the CH<sub>3</sub>-FR modes. Spectral fits using Lorentzian functions (IGOR, version 4.0.5.1, Lorentzian fitting function written to incorporate phase) for the BBSFG spectrum is also shown in Figure 2, the individual peaks and the additive calculated spectrum, which also includes the phase relationships. Different from the Raman peak fits shown in Figure 1 where a Voigt function was utilized,

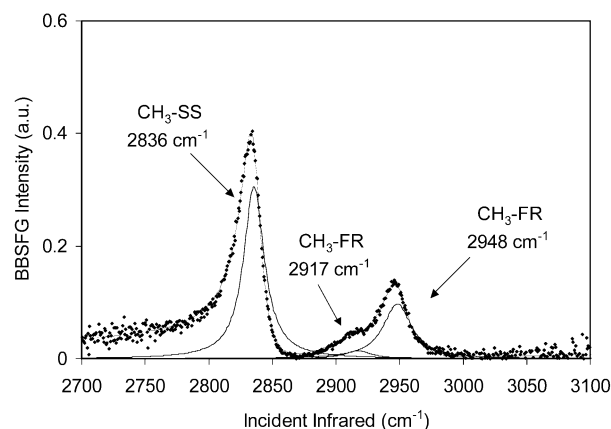


**Figure 2.** BBSFG spectrum from the air–liquid interface of neat methanol (CH<sub>3</sub>OH). The 2917 cm<sup>-1</sup> peak is magnified 10 times. The solid lines are the calculated Lorentzian fits.

the SFG spectrum shown in Figure 2 was fit to a solely Lorentzian profile. The convolution of Lorentzian and Gaussian line shapes, the Voigt profile, fit the SFG spectra unsatisfactorily. Thus the calculated fit to the BBSFG spectrum of neat methanol was completed using eqs 1 and 2. The best fitting result was obtained by using three Lorentzian peaks of the same phase with out-of-phase nonresonant terms. The BBSFG peak fitting parameters are shown in Table 2. As shown in Figure 2, the calculated spectral fit, the solid line that passes through the data in Figure 2, overlays the experimental data very well.

Randomly oriented methanol molecules would result in an average zero surface macroscopic susceptibility (i.e., cancellation of SFG signal), as revealed from eq 3, and oriented molecules relative to one another would provide a net SFG signal. The observed BBSFG spectrum from the air–methanol interface, in particular the strong SFG response from the CH<sub>3</sub>-SS, as shown in Figure 2, is indicative of a net orientation of the methanol molecules at the surface as one might expect at this interface. Methanol is a strong hydrogen-bonding agent, and hydrogen bonding influences the structural properties of methanol to a great extent. Molecular dynamic studies indicate that the net ordering at the surface of neat methanol solutions can be understood as a result of placing the hydrophobic methyl group toward the vapor phase to maximize the number of hydrogen bonds near the surface, which then minimizes the surface energy.<sup>35</sup> Thus, hydrogen bonding can be considered as a significant driving force for the orientation of methanol molecules at the surface of neat methanol.

To further understand the influence of hydrogen bonding on the surface structure of methanol solutions, a series of aqueous methanol solutions were investigated using BBSFG spectroscopy. BBSFG spectra of five methanol solutions at the bulk

**TABLE 2: Fitting Results of the BBSFG Spectra in the C–H Stretch Region of Aqueous Methanol (CH<sub>3</sub>OH) Solutions<sup>a</sup>**

mole fraction	CH <sub>3</sub> -SS				CH <sub>3</sub> -FR (1); CH <sub>3</sub> -FR (2)				$\chi_{nr}$ Re; Im (a.u.)
	$\nu$ (cm <sup>-1</sup> )	$A_\nu$ (a.u.)	$I_\nu$ (a.u.)	$\Gamma$ (cm <sup>-1</sup> ) HWHM	$\nu$ (cm <sup>-1</sup> )	$A_\nu$ (a.u.)	$I_\nu$ (a.u.)	$\Gamma$ (cm <sup>-1</sup> ) HWHM	
0.03	2843	2.8	2.6	8.7	2925; 2955	0.28; 2.3	0.02; 1.6	13; 9.9	-0.10; -0.017
0.06	2841	3.8	4.5	9.3	2925; 2953	0.64; 3.0	0.09; 2.5	14; 11	-0.087; -0.012
0.14	2840	5.2	8.3	9.6	2924; 2951	0.63; 4.2	0.11; 4.1	10; 11	-0.10; -0.021
0.19	2839	6.2	11.6	9.7	2925; 2950	1.3; 4.7	0.34; 5.8	14; 11	-0.098; -0.011
0.36	2838	6.6	13.1	9.7	2923; 2950	1.1; 5.2	0.28; 6.5	12; 12	-0.11; -0.015
0.57	2837	6.7	13.2	9.9	2921; 2948	1.8; 4.9	0.56; 5.8	16; 12	-0.099; 0.005
0.69	2837	6.5	12.3	10	2922; 2948	1.7; 4.9	0.48; 5.6	17; 12	-0.10; 0.008
0.83	2837	6.1	10.8	10	2919; 2948	0.9; 4.9	0.20; 5.1	12; 13	-0.11; -0.014
1.0	2836	5.4	8.7	9.8	2917; 2948	0.48; 4.2	0.05; 3.7	13; 14	-0.13; -0.032

<sup>a</sup>  $\nu$ : peak frequency;  $A_\nu$ : peak amplitude;  $I_\nu$ : peak intensity (integrated peak area);  $\Gamma$  (HWHM): half width at half-maximum;  $\chi_{nr}$ : nonresonant term; Re: real part; Im: imaginary part; signs of  $A_\nu$  and  $\chi_{nr}$  denote the phases.

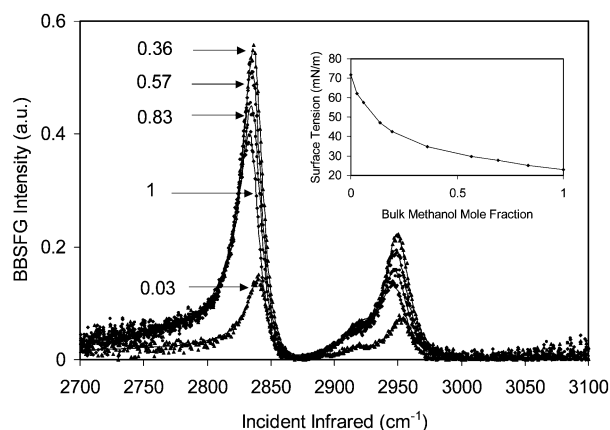


**Figure 3.** BBSFG spectra of aqueous methanol (CH<sub>3</sub>OH) solutions at different bulk methanol mole fractions. Symbols are the experimental data points; solid lines are the calculated fits. Inset: surface tension of aqueous methanol solutions at different bulk methanol mole fractions at 25 °C.

methanol mole fractions of 0.03, 0.36, 0.57, 0.83, and 1.0 are shown in Figure 3. A total of 8 aqueous methanol solutions were investigated using BBSFG. For simplicity, only 4 of these solution spectra are shown. These spectra reveal the dominant trends with respect to spectral shift and SFG intensity changes. In addition, we have completed Raman studies of these same solutions to clarify the role that the surface plays in comparison to the bulk hydrogen-bonding effects. The Raman spectra of the CH region of a representative set of aqueous methanol solutions are shown in Figure 4. In the inset of Figure 4, the Raman spectrum for the 0.36 mole fraction methanol solution is shown with a Voigt fit, including the individual peaks contributing to this fit. In the fit for the Raman spectra of the aqueous solutions, it was necessary to include the OH bonding region to properly fit the CH peaks due to the overlap of spectral tails as shown in the inset of Figure 4. Fitting results of the Raman spectra for the CH modes are shown in Table 1.

The spectral peak assignments of the BBSFG spectra of the methanol solutions shown in Figure 3 are the same as those assigned to the neat methanol solution (Figure 2), although the peak positions change with concentration changes. The BBSFG peak position changes are shown in Figure 5. Three Lorentzian peaks were used to calculate the spectral fits including the peak positions, and as shown in Figure 3, the calculated fits overlay the experimental data quite well. Fitting parameters for these fits are shown in Table 2. Typically, all parameters were allowed to vary. The frequency of the BBSFG CH<sub>3</sub>-SS peak position decreases (red-shifts) from 2843 to 2836 cm<sup>-1</sup> with increasing methanol concentration, bulk, and surface mole fractions. The

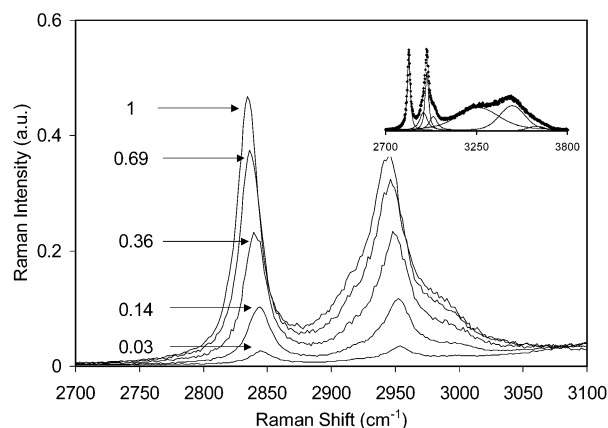


**Figure 4.** Raman spectra of aqueous methanol (CH<sub>3</sub>OH) solutions at different bulk methanol mole fractions. Inset: experimental data and calculated fit for the 0.36 methanol mole fraction solution in the CH and OH spectral regions.

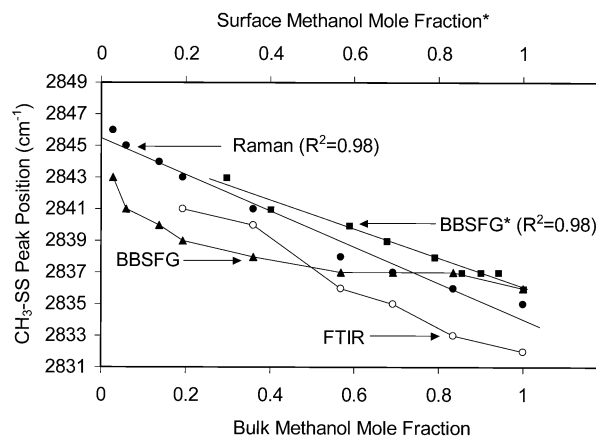


**Figure 5.** The CH<sub>3</sub>-SS peak positions for Raman, FTIR, and BBSFG data as a function of methanol (CH<sub>3</sub>OH) mole fraction. Raman denotes the Raman peak position versus the bulk mole fraction; FTIR denotes the FTIR peak position versus the bulk mole fraction where the line is a guide to the eye; BBSFG\* denotes the BBSFG peak position versus surface mole fraction (normalized surface number density); BBSFG denotes the BBSFG peak position versus bulk mole fraction where the line is a guide to the eye. Lines for the Raman and BBSFG\* are linear fits to the data.

changes in the BBSFG CH<sub>3</sub>-SS peak positions (triangle data points in Figure 5) observed from the aqueous methanol solution surfaces do not follow a simple linear relationship with bulk mole fraction. Since methanol molecules are surface active relative to water molecules in aqueous methanol solutions, the bulk mole fraction does not directly reflect the mole fraction



of methanol at the surface of its aqueous solutions. Thus, using previously published surface number density data<sup>29,36</sup> for aqueous methanol solutions, the normalized surface number density (surface mole fraction) is also used here for comparison and is shown as the top axis in Figure 5. As shown in Figure 5, the CH<sub>3</sub>-SS peak positions for the BBSFG spectra (BBSFG\* square data points) relative to the surface concentration (top axis) also show a decrease in frequency upon increasing methanol concentration. However, the relationship is relatively linear with respect to the surface mole fraction as is shown by the linear fit ( $R^2 = 0.98$ ). The Raman CH<sub>3</sub>-SS peak positions (circular data points) versus bulk methanol concentration (bottom axis) are also shown in Figure 5 for comparison. The Raman data show a linear relationship with bulk mole fraction ( $R^2 = 0.98$ ). The 3 sets of data shown in Figure 5 similarly reveal a red-shift in the CH<sub>3</sub>-SS frequency upon increase of methanol concentration (i.e., blue-shift with increasing water concentration). The trend is strikingly linear for the Raman as well as the BBSFG\* data when comparisons are made to the adjusted mole fraction for the BBSFG\* data (the normalized surface number density data denoted as surface mole fraction, i.e., BBSFG\*). Although the Raman and BBSFG\* data are similar, the BBSFG\* CH<sub>3</sub>-SS peak frequencies are blue-shifted (reside at higher frequencies) relative to the Raman peak frequencies for the respective local concentration. To verify the relative blue-shift, a series of FTIR spectra of the methanol solutions were obtained since the BBSFG peak position of the vibrational mode is determined not only by the corresponding Raman peak position, but also by the infrared peak position. The IR results are also shown in Figure 5. With the methanol bulk concentration increasing from 0.19 to 1.0 mole fraction, the CH<sub>3</sub>-SS peak frequencies decrease from 2841 to 2832 cm<sup>-1</sup>. The infrared peak position is further red-shifted relative to the respective Raman peak positions. Therefore, the BBSFG\* data is blue-shifted relative to the respective bulk vibrational data, Raman, and FTIR.

The peak position changes of the CH<sub>3</sub>-SS in the Raman, FTIR, and the BBSFG spectra can be explained from the viewpoint of changing hydrogen-bonding configurations. The CH<sub>3</sub>-SS is a relatively sensitive probe of hydrogen bonding within methanol solutions.<sup>33,37</sup> Resonant ion-dip infrared spectroscopy investigations of methanol-containing clusters indicated that the CH<sub>3</sub>-SS is sensitive to the variation of the local hydrogen-bonding environment. Density functional theory (DFT) calculation further indicated that methanol may act as a hydrogen-acceptor (A) causing a blue-shift of the CH<sub>3</sub>-SS frequency; however, a red-shift occurs when methanol acts as a hydrogen-donor (D). Additionally, the frequency shift from accepting two hydrogens is more extreme in the observed blue-shift.<sup>33</sup> Both experiment and theoretical studies indicate that shifts as much as 30 cm<sup>-1</sup> might be observed from methanol-containing clusters.<sup>33</sup>

In the Raman, FTIR, and BBSFG studies presented here, with the decrease of water concentration (i.e., increasing methanol mole fraction) the red-shift that we observe at the surface and in the bulk is indicative of methanol becoming a more efficient hydrogen donor. Or said another way, as the water content increases, methanol molecules are more efficient at accepting hydrogen from neighboring water molecules.

As stated above, the Raman and BBSFG\* peak frequency data shown in Figure 5 are similarly linear (as well as the IR), however, the BBSFG\* CH<sub>3</sub>-SS peak frequencies reside at higher frequencies relative to the Raman and IR peak frequencies for their respective local concentration. Raman and IR spectroscopy

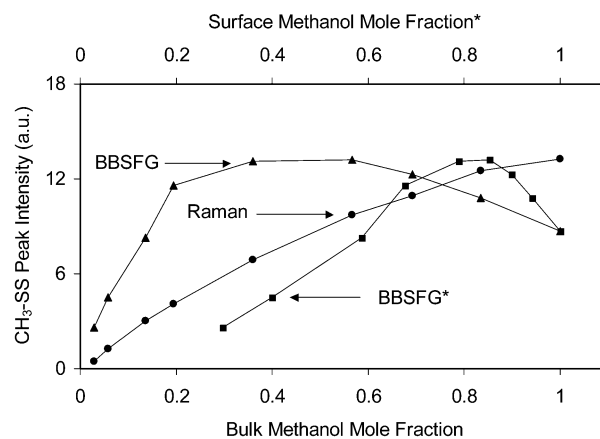


**Figure 6.** CH<sub>3</sub>-SS peak intensities (peak areas) as a function of methanol mole fraction. BBSFG denotes the BBSFG peak intensity versus bulk methanol mole fraction; Raman denotes the Raman peak intensity versus the bulk methanol mole fraction; BBSFG\* denotes the BBSFG peak intensity versus surface methanol mole fraction. (Lines are only guides to the eye.)

probes the bulk 3-dimensional solvation environment, whereas the BBSFG spectroscopy probes the surface approximate 2-dimensional solvation environment. Thus, differences in the CH<sub>3</sub>-SS peak frequency might be expected. Our observed blue-shift of the BBSFG\* data can be explained by the hydrogen-bonding model discussed above. That is, the hydrogen bonding character of methanol is affected by the local environment, particularly at an interface. Just as in the bulk, when there are more water molecules available for hydrogen bonding to methanol OH groups, a blue-shift is observed. The observed blue-shift of the CH<sub>3</sub>-SS from the BBSFG\* data suggests that the methanol molecules existing in the surface region have a higher tendency of accepting hydrogen relative to the bulk environment. This blue-shift is consistent with the hydrogen-acceptor model.<sup>33</sup> Consistent with our interpretation, the hydrogen-bonding interaction between water and methanol at the aqueous methanol surface has been observed directly using scanning SFG via the loss of the surface dangling OH of water.<sup>38</sup> Additionally, theoretical studies support the hydrogen bonding influence of methanol on the surface dangling OH of water.<sup>39</sup> This can be further elucidated in that the methanol molecules existing in the surface region have a higher tendency of accepting hydrogen relative to the bulk environment. The surface activity of methanol molecules in an aqueous environment drive the CH<sub>3</sub> group into the hydrophobic or air phase as the OH of the methanol is efficiently solvated by the water molecules in the surface and subsurface region.

Further analysis on the Raman and BBSFG spectra of the methanol solutions, neat and aqueous, shown in Figures 1–4, reveal distinctly different intensity trends. We focus on the CH<sub>3</sub>-SS since the transition moment of the CH<sub>3</sub>-SS in BBSFG using ssp polarizations characterizes the orientation of the methanol at the air–liquid interface. As shown in Figure 6, Raman peak intensities (i.e., integrated peak areas) of the CH<sub>3</sub>-SS increase with increasing mole fraction of methanol (see Figure 4 and Table 1). The Raman intensity increase, although not strictly linear, is consistent with the increase in the number of methanol molecules within the bulk solution. Also shown in Figure 6, the BBSFG CH<sub>3</sub>-SS peak intensities (i.e., integrated areas) with increasing methanol bulk mole fraction have a more atypical shape. The BBSFG CH<sub>3</sub>-SS peak intensities increase to a maximum at 0.57 methanol bulk mole fraction and then slowly decrease to approximately 70% of the maximum intensity value. The BBSFG\* CH<sub>3</sub>-SS peak intensities more correctly compared

to the surface mole fraction have more physical relevance. These data also shown in Figure 6 (square data points versus the top  $X$  axis) reveal that the maximum BBSFG\* intensity for the  $\text{CH}_3$ -SS resides at a surface methanol mole fraction of  $\sim 0.8$  (4 methanol molecules for every 1 water molecule). The BBSFG\* intensity is then shown to decrease to  $\sim 70\%$  of the maximum intensity value.

A reasonable explanation for the Raman  $\text{CH}_3$ -SS intensity changes observed in Figure 6 is the changing solvation effects and possible decreases in the transition moment strength as the methanol concentration increases. Yet the BBSFG  $\text{CH}_3$ -SS intensity changes are clearly indicative of methanol orientation changes in the surface region. Recall that SFG is surface-selective and is sensitive to both the surface number density as well as orientation. The transition moment strength will also modify the SFG response to the number density, which will be similar to the effect on the Raman response. As indicated in eq 3, the SFG intensity of a surface vibrational mode is related to surface number density  $N$ , surface orientation  $\langle \mu_{IJK:lmn} \rangle$ , and the molecular hyperpolarizability,  $\beta_v$ . Therefore, if the surface number density is playing a dominating role in eq 3, the SFG intensity will continually increase with the increase of surface mole fraction of methanol. However, Figure 6 clearly shows that this is not the case for the BBSFG  $\text{CH}_3$ -SS intensities. For example, there must be other opposing factors, which offset the surface number density's impact on the SFG intensity in the high mole fraction region (surface mole fraction  $> 0.8$ ). In this case, considering that the molecular hyperpolarizability  $\beta_v$  may be weakly dependent on concentration, a likely factor may be the orientation average term  $\langle \mu_{IJK:lmn} \rangle$  in eq 3. With ssp polarization, the SFG intensity of the  $\text{CH}_3$ -SS will be weaker if the  $\text{CH}_3$ -SS transition moment vector is at a larger orientation angle  $\theta$  relative to the surface normal, yet stronger at smaller orientation angles as shown in eq 4.<sup>19</sup>

$$\chi_{yyz} \propto \beta_{nnn} [\cos \theta (1 + \gamma) - \cos^3 \theta (1 - \gamma)], \gamma = \beta_{lll}/\beta_{nnn} \quad (4)$$

Therefore, it can be deduced from Figure 6 that in the high mole fraction region (surface mole fraction  $> 0.8$ ) with the increase of methanol concentration the methanol molecules need to reorient from smaller  $\theta$  to larger  $\theta$  on average in order to offset the surface number density effect on the SFG intensity. Conclusively, surface methanol molecules change their average orientational configuration throughout the full concentration range. At concentrations above 0.8 surface methanol mole fraction (0.57 bulk mole fraction), the methanol molecules in the surface region may lie closer to the surface plane and/or have a larger distribution of angles relative to the surface normal, suggesting a somewhat disordered surface. The average orientation angle of the  $\text{CH}_3$ -SS transition moment of methanol molecules relative to the surface normal from a neat methanol solution surface has been calculated to be less than 60 degrees;<sup>40</sup> although this measurement has been disputed,<sup>29</sup> it is consistent with our interpretation of a relatively low amount of order and broad orientation distribution for high concentrations of methanol. Additionally important, the changing surface hydrogen-bonding environment, particularly due to the lack of surface water molecules, is likely playing a significant role in the changing surface orientation of the methanol molecules in the high concentration regime.

One possible argument with the origin of the BBSFG intensity change is that the BBSFG intensity of the  $\text{CH}_3$ -SS can be affected by the resonant SFG response from the OH symmetric stretch (OH-SS) of  $\text{H}_2\text{O}$  and the OH stretch of  $\text{CH}_3\text{OH}$  since

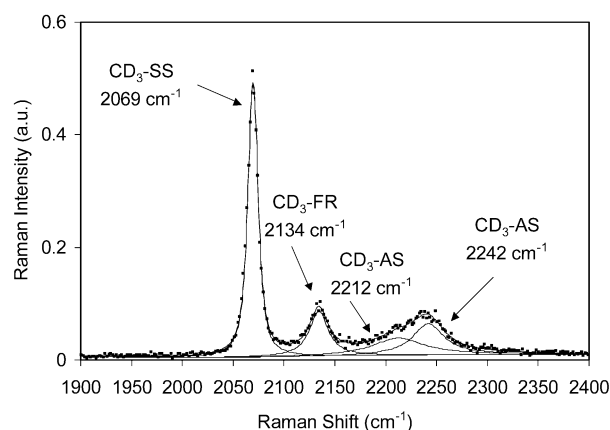


**Figure 7.** Raman spectrum of neat partially deuterated methanol ( $\text{CD}_3\text{OH}$ ).  $\text{CD}_3$ -SS:  $\text{CD}_3$  symmetric stretch;  $\text{CD}_3$ -FR:  $\text{CD}_3$  Fermi resonance;  $\text{CD}_3$ -AS:  $\text{CD}_3$  asymmetric stretch. The solid lines are the calculated Voigt fits.

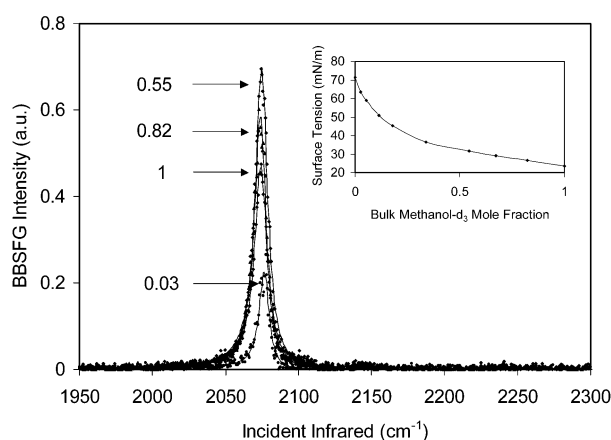


**Figure 8.** BBSFG spectra of aqueous partially deuterated methanol ( $\text{CD}_3\text{OH}$ ) solutions at different bulk methanol mole fractions. Symbols are the experimental data points; solid lines are the calculated fits. Inset: surface tension of aqueous methanol solutions at different bulk methanol mole fractions at 28 °C.

the  $\text{CH}_3$ -SS and the OH stretches overlap spectrally to some extent. Since SFG is a coherent process, either an in-phase or out-of-phase relationship between the  $\text{CH}_3$ -SS and the OH stretches can dramatically affect the BBSFG intensity of the  $\text{CH}_3$ -SS. To further clarify the origin of the BBSFG intensity change of the  $\text{CH}_3$ -SS mode, partially deuterated methanol ( $\text{CD}_3\text{OH}$ ) aqueous solutions were studied. Figure 7 shows the Raman spectrum of neat  $\text{CD}_3\text{OH}$ , as well as the Voigt-function fitting and peak assignments. The  $\text{CD}_3$ -SS peak position is located at  $\sim 2069 \text{ cm}^{-1}$ , which is far away from the OH stretching region. There is no overlap between the  $\text{CD}_3$  stretching modes and the OH stretching modes. As illustrated in the inset of Figure 3 and the inset of Figure 8,  $\text{CH}_3\text{OH}$  and  $\text{CD}_3\text{OH}$  surface tension data follow similar trends, indicating that the surface number density of  $\text{CD}_3\text{OH}$  also increases with the increase of bulk mole fraction. Figure 8 shows several BBSFG spectra of the air-liquid interface of the  $\text{CD}_3\text{OH}-\text{H}_2\text{O}$  system taken with an ssp polarization combination. Although the fs IR energy covers the  $1850 \text{ cm}^{-1}$  to  $2300 \text{ cm}^{-1}$  region, only the  $\text{CD}_3$ -SS at  $\sim 2074 \text{ cm}^{-1}$  is clearly observed from the BBSFG spectra. As shown in Figure 8, with the bulk  $\text{CD}_3\text{OH}$  mole fraction increasing from 0.55 to 1.0, which coincides with an increase of the methanol surface number density, the BBSFG intensity decreases, which confirms the  $\text{CH}_3\text{OH}$  results. In addition, the BBSFG peak frequency change of the  $\text{CD}_3$ -SS

in the CD<sub>3</sub>OH–H<sub>2</sub>O system is similar to that of the CH<sub>3</sub>OH–H<sub>2</sub>O system.

## Conclusions

The air–liquid interfaces and solutions of aqueous methanol mixtures were studied using vibrational broad bandwidth sum frequency generation, Raman and FTIR spectroscopy, respectively, in the CH and CD vibrational regions. The CH<sub>3</sub>-SS peak position shifts observed in the surface and bulk studies were explained by invoking a hydrogen-bonding model in that when less water molecules are available to solvate the methanol OH, methanol acts as an efficient hydrogen donor. Interestingly, the CH<sub>3</sub>-SS frequencies of surface methanol in the BBSFG spectra were found to be blue-shifted relative to the frequencies observed for this mode in the bulk solution studied by Raman and FTIR spectroscopy. This indicates that methanol at the surface of its respective solution has an increased tendency to accept hydrogen from the surface and subsurface water molecules relative to this propensity in the bulk. Additional studies of the intensities of the CH<sub>3</sub>-SS of methanol at the surface as a function of methanol concentration revealed that the surface methanol molecules become less ordered (i.e., broader orientation angle distribution) at bulk methanol mole fractions above 0.57. This was further verified from the BBSFG study of the partially deuterated methanol (CD<sub>3</sub>OH) aqueous solutions.

**Acknowledgment.** We acknowledge The Ohio State University and the National Science Foundation through The Ohio State University Environmental Molecular Science Institute for funding (NSF Grant No. CHE-0089147). We additionally acknowledge the National Science Foundation for funding through the NSF CAREER Award (NSF Grant No. CHE-0134131).

## References and Notes

- (1) Singh, H. B.; Kanakidou, M.; Crutzen, P. J.; Jacob, D. J. *Nature* **1995**, *378*, 50–54.
- (2) Singh, H.; Chen, Y.; Staudt, A.; Jacob, D.; Blake, D.; Heikes, B.; Snow, J. *Nature* **2001**, *410*, 1078–1081.
- (3) Hudson, P. K. Z.; Mark A.; Tolbert, Margaret A. *J. Phys. Chem. A* **2002**, *106*, 2882–2888.
- (4) Singh, H.; Chen, Y.; Tabazadeh, A.; Fukui, Y.; Bey, I.; Yantosca, R.; Jacob, D.; Arnold, F.; Wohlfrom, K.; Atlas, E.; Flocke, F.; Blake, D.; Blake, N.; Heikes, B.; Snow, J.; Talbot, R.; Gregory, G.; Sachse, G.; Vay, S.; Kondo, Y. *J. Geophys. Res.* **2000**, *105*, 3795–3805.
- (5) Jaegle, L.; Jacob, D. J.; Brune, W. H.; Faloona, I.; Tan, D.; Heikes, B. G.; Kondo, Y.; Sachse, G. W.; Anderson, B.; Gregory, G. L.; Singh, H. B.; Pueschel, R.; Ferry, G.; Blake, D. R.; Shetter, R. E. *J. Geophys. Res.* **2000**, *105*, 3877–3892.
- (6) Ma, G.; Allen, H. C. *J. Am. Chem. Soc.* **2002**, *124*, 9374–9375.
- (7) Briggman, K. A.; Stephenson, J. C.; Wallace, W. E.; Richter, L. J. *J. Phys. Chem. B* **2001**, *105*, 2785–2791.
- (8) Richter, L. J.; Petralli-Mallow, T. P.; Stephenson, J. C. *Opt. Lett.* **1998**, *23*, 1594–1596.
- (9) Miranda, P. B.; Shen, Y. R. *J. Phys. Chem. B* **1999**, *103*, 3292–3307.
- (10) Gragson, D. E.; Richmond, G. L. *J. Phys. Chem. B* **1998**, *102*, 3847–3861.
- (11) Opdahl, A.; Phillips, R. A.; Somorjai, G. A. *Macromolecules* **2002**, *35*, 4387–4396.
- (12) Eisenthal, K. B. *Chem. Rev.* **1996**, *96*, 1343–1360.
- (13) Allen, H. C.; Raymond, E. A.; Richmond, G. L. *Curr. Opin. Colloid Interface Sci.* **2000**, *5*, 74–80.
- (14) Allen, H. C.; Raymond, E. A.; Richmond, G. L. *J. Phys. Chem.* **2001**, *105*, 1649–1655.
- (15) Schnitzer, C.; Baldelli, S.; Campbell, D. J.; Shultz, M. J. *J. Phys. Chem. A* **1999**, *103*, 6383–6386.
- (16) Schnitzer, C.; Baldelli, S.; Shultz, M. J. *J. Phys. Chem. B* **2000**, *104*, 585–590.
- (17) Raduege, C.; Pflumio, V.; Shen, Y. R. *Chem. Phys. Lett.* **1997**, *274*, 140–144.
- (18) Shen, Y. R. *The Principles of Nonlinear Optics*, 1st ed.; John Wiley & Sons: New York, 1984.
- (19) Zhuang, X.; Miranda, P. B.; Kim, D.; Shen, Y. R. *Phys. Rev. B* **1999**, *59*, 12632–12640.
- (20) Bain, C. D. *J. Chem. Soc., Faraday Trans.* **1995**, *91*, 1281–1296.
- (21) Wolfrum, K.; Laubereau, A. *Chem. Phys. Lett.* **1994**, *228*, 83–88.
- (22) Dick, B.; Gierulski, A.; Marowsky, G. *Appl. Phys. B* **1985**, *38*, 107–116.
- (23) Hirose, C.; Akamatsu, N.; Domen, K. *Appl. Spectrosc.* **1992**, *46*, 1051–1072.
- (24) Morita, A.; Hynes, J. T. *Chem. Phys.* **2000**, *258*, 371–390.
- (25) Heinz, T. F. In *Nonlinear surface electromagnetic phenomena*; Ponath, H.-E., Stegeman, G. I., Eds.; Elsevier Science Publishers: North-Holland, Amsterdam, 1991; pp 353–416.
- (26) Hommel, E. L.; Ma, G.; Allen, H. C. *Anal. Sci.* **2001**, *17*, 1325–1329.
- (27) Hommel, E. L.; Allen, H. C. *Anal. Sci.* **2001**, *17*, 137–139.
- (28) Stanners, C. D.; Du, Q.; Chin, R. P.; Cremer, P.; Somorjai, G. A.; Shen, Y. R. *Chem. Phys. Lett.* **1995**, *232*, 407–413.
- (29) Wolfrum, K.; Graener, H.; Laubereau, A. *Chem. Phys. Lett.* **1993**, *213*, 41–46.
- (30) Schwartz, M.; Moradi-Araghi, A.; Koehler, W. H. *J. Mol. Struct.* **1980**, *63*, 279–285.
- (31) Schwartz, M.; Moradi-Araghi, A.; Koehler, W. H. *J. Mol. Struct.* **1982**, *81*, 245–252.
- (32) Bertie, J. E.; Zhang, S. L. *J. Mol. Struct.* **1997**, *413–414*, 333–363.
- (33) Gruenloh, C. J.; Florio, G. M.; Carney, J. R.; Hagemester, F. C.; Zwier, T. S. *J. Phys. Chem. A* **1999**, *103*, 496–502.
- (34) Halonen, L. *J. Chem. Phys.* **1997**, *106*, 7931–7945.
- (35) Matsumoto, M.; Kataoka, Y. *J. Chem. Phys.* **1989**, *90*, 2398–2407.
- (36) Kipling, J. J. *J. Colloid Sci.* **1963**, *18*, 502–511.
- (37) Dixit, S.; Poon, W. C. K.; Crain, J. J. *Phys.: Condens. Matter* **2000**, *12*, L323–L328.
- (38) Du, Q.; Freysz, E.; Shen, Y. R. *Science* **1994**, *264*, 826–828.
- (39) Benjamin, I. *Phys. Rev. Lett.* **1994**, *73*, 2083–2086.
- (40) Superfine, R.; Huang, J. Y.; Shen, Y. R. *Phys. Rev. Lett.* **1991**, *66*, 1066–1069.